Eur. Phys. J. Plus (2023) 138:1026
https://doi.org/10.1140/epjp/s13360-023-04594-x

THE EUROPEAN PHYSICAL JOURNAL PLUS

Regular Article

# Electronic and optical properties of the exponential and hyperbolic Rosen–Morse types quantum wells under applied magnetic field

**E. Kasapoglu**[1], **M. B. Yücel**[2,a], **C. A. Duque**[3,b]

[1] Department of Physics, Faculty of Science, Sivas Cumhuriyet University, 58140 Sivas, Türkiye
[2] Department of Physics, Faculty of Science, Akdeniz University, 07058 Antalya, Türkiye
[3] Grupo de Materia Condensada-UdeA, Instituto de Física, Facultad de Ciencias Exactas y Naturales, Universidad de Antioquia UdeA, Calle 70 No. 52-21, Medellín, Colombia

Received: 12 August 2023 / Accepted: 13 October 2023


**Abstract** In this study, we considered the electronic and optical properties of quantum wells with the exponential and hyperbolic Rosen–Morse potentials under an applied magnetic field. Calculations are made within the framework of effective mass and parabolic band approximations. We have used the diagonalization method by choosing a wave function based on the trigonometric orthonormal function to find eigenvalues and eigenfunctions of the confined electron. Our results show that the magnetic field, asymmetry, and confinement parameters cause a significant increase in electron energies and energy differences between the electron states and the blue shift in the absorption peaks. These results can be used to probe materials' electronic and structural properties and develop new materials with tailored optical properties.

## 1 Introduction

Semiconductor quantum wells (QWs) have attracted much interest due to their promising potential applications in electronic and optoelectronic devices. In these nanostructures, the quantum confinement effects on the charge carriers have quite different electronic and optical properties than their bulk materials [1]. External perturbations, such as electric, magnetic, or intense laser fields, are powerful tools in controlling the optical response of low-dimensional semiconductor systems.

Thanks to recent advancements in material growth techniques, due to their unusual electronic and optical properties, single or multiple QWs consisting of inhomogeneous pieces with various confinement potentials have attracted remarkable attention. These structures' electronic and optical properties can be adjusted according to the desired outcome by selecting appropriate geometries, material parameters, and applied external fields, leading to new potential applications in optoelectronics. Therefore, these structures have been extensively studied and are still being investigated under external fields such as electric, magnetic, and intense laser fields [2–18].

The main objective of selecting the appropriate confinement potential profile for any of the mentioned structures is to manipulate their electronic properties to best reflect the material's atomic structure and enable the design of new optoelectronic devices. It should be noted that the physics of QWs with different confinement potentials offers opportunities to explore new applications in lower dimensions. In addition to the different shaped QWs mentioned above, molecular potentials such as Konwent [19], Manning [20], hyperbolic type Rosen–Morse [21–23], and Razavy [24] are used extensively in the investigation of electronic and optical properties of low-dimensional systems.

The exponential Rosen–Morse potential has independent fitting parameters more than the hyperbolic type Rosen–Morse potential for the experimental results. The exponential Rosen–Morse quantum well (eRMQW) is a more reliable and advantageous model as it provides a more flexible framework than the hyperbolic type Rosen–Morse potential, which includes more parameters to represent experimental data accurately. Although there are a limited number of studies on the optical properties of QWs and quantum dots with hyperbolic type Rosen–Morse potential under external fields [21–23], as far as we know, one has not reported any investigation on the electronic and optical properties of the eRMQW except for the calculation of rotational vibration energies of some diatomic molecules. Therefore, in this study, we investigated, for the first time, the electronic and optical properties of the eRMQW under an applied magnetic field. In addition, in order to make a detailed comparison with the hyperbolic RMQW (hRMQW) potential, the hRMQW potential function modified by us was defined, and both QWs were investigated in detail, and the results were compared.

[a] e-mail: myucel@akdeniz.edu.tr
[b] e-mail: carlos.duque1@udea.edu.co (corresponding author)

Published online: 18 November 2023

This work is arranged as follows: The theoretical framework is presented in Sect. 2, the results and discussion are outlined in Sect. 3, and the conclusions are given in Sect. 4.

## 2 Theoretical model

In the effective mass approximation, the Hamiltonian for an electron under the magnetic field can be expressed as follows:

$$H = \frac{1}{2\,m^*}\left[\vec{p} + \frac{e}{c}\,\vec{A}(\vec{r})\right]^2 + V(z) \tag{1}$$

or

$$H = -\frac{\hbar^2}{2\,m^*}\,\frac{d^2}{d\,z^2} + \frac{e^2\,B^2\,z^2}{2\,m^*\,c^2} + V(z)\,, \tag{2}$$

where the magnetic field ($\vec{B}$) is applied perpendicular to the growth direction,$\vec{A}(\vec{r})$ is the vector potential, and it is written in the form $\vec{A}(\vec{r}) = (0,\ -B\,z,\ 0)$ to describe the applied magnetic field; $\vec{p}$ is the momentum operator, $m^*$ is the electron effective mass, $e$ is the elementary charge, and $V(z)$ is the confinement potential of the eRMQW; its functional form is given as follows [25]:

$$V^{eRMQW}(z) = V_0\left(1 - \frac{e^{z_0/k}+1}{e^{z/k}+1}\right)^2, \tag{3}$$

where $V_0$ is the QW depth, the $k$-parameter is related to the well-width, and $z_0$ is the $z$-position of the minimum point of the potential, it is also the distance from the equilibrium position and also affects the well-width. It should also be noted that using the eRM potential used in the literature to obtain the molecular energy spectrum of diatomic molecules has been modified by us to investigate the electronic and optical properties of an electron confined within this potential.

Immediately after the energies and related wavefunctions are acquired, linear and nonlinear absorption coefficients are found for transitions between two electronic states using the perturbation expansion and the density matrix methods. Using the relevant approaches mentioned before, expressions of the linear, third-order nonlinear, and total absorption coefficients (TACs) for the optical transitions are found as follows [18, 19, 26, 27], respectively:

$$\beta^{(1)}(\omega) = \sqrt{\frac{\mu_0}{\varepsilon_r}}\,\frac{\left|M_{ij}\right|^2\sigma_v\hbar\omega\Gamma_{ij}}{(E_{ij}-\hbar\omega)^2+(\hbar\Gamma_{ij})^2}, \tag{4}$$

$$\beta^{(3)}(\omega, I) = -2\sqrt{\frac{\mu_0}{\varepsilon_r}}\left(\frac{I}{\varepsilon_0 n_r c}\right)\frac{\left|M_{ij}\right|^2\sigma_v\hbar\omega\Gamma_{ij}}{(E_{ij}-\hbar\omega)^2+(\hbar\Gamma_{ij})^2}$$

$$\left(1 - \frac{\left|M_{jj}-M_{ii}\right|^2}{\left|2M_{ij}\right|^2}\,\frac{(E_{ij}-\hbar\omega)^2-(\hbar\Gamma_{ij})^2+E_{ij}(E_{ij}-\hbar\omega)}{E_{ij}^2+(\hbar\Gamma_{ij})^2}\right), \tag{5}$$

and

$$\beta(\omega, I) = \beta^{(1)}(\omega) + \beta^{(3)}(\omega, I)\,, \tag{6}$$

where $\varepsilon_r = n_r^2\varepsilon_0$ is the real part of the permittivity, $\sigma_v$ is the carrier density in the system, $\mu_0$ is the vacuum permeability, $E_{ij} = E_j - E_i$ is the energy difference between two impurity states, $M_{ij} = \left|\langle\psi_i|ez|\psi_j\rangle\right|$, $(i,\ j\ =\ 1,\ 2)$ is the transition matrix element between the eigenstates $\psi_i$ and $\psi_j$ for incident radiation polarized in the z-direction, $\Gamma_{ij}(= 1/T_{ij})$ is the relaxation rate, $T_{ij}$ is the relaxation time, $c$ is the speed of the light in free space, and $I$ is the intensity of incident photon with the $\omega$-angular frequency that leads to the intersubband optical transitions. It should be noted that diagonal (non-diagonal) matrix elements are zero (different zero) $M_{ii} = M_{jj} = 0$,$(M_{ij} \neq 0)$ in the symmetric case for $z_0 = 0$.

## 3 Results and discussion

The parameter values in our numerical calculations are $\epsilon = 12.58$, $m^* = 0.067m_0$ (where $m_0$ is the free electron mass), $V_0 = 228$ meV, $n_r = \sqrt{\epsilon} = 3.55$, $T_{12} = 0.4\ ps$, $\Gamma_{12} = 1/T_{12}$, $\mu_0 = 4\pi \times 10^{-7}$ Hm$^{-1}$, $\sigma_v = 3.0 \times 10^{22}$ m$^{-3}$, and $I = 5.0 \times 10^8$ W/m$^2$. These parameters suit for GaAs/GaAlAs heterostructures [13].

The presentation of results has been divided into two subsections. In subsection A, attention is focused on the eRMQW, giving greater relevance to the $z_0$-parameter and the dimensions of the structure, associated with the $k$-parameter. The results are given for zero and 10 T of the magnitude of the applied magnetic field. In subsection B, a comparison is made of the results for the eRMQW and the hRMQW as a function of the applied magnetic field, considering a fixed value of the $z_0$ and $k$-parameters.

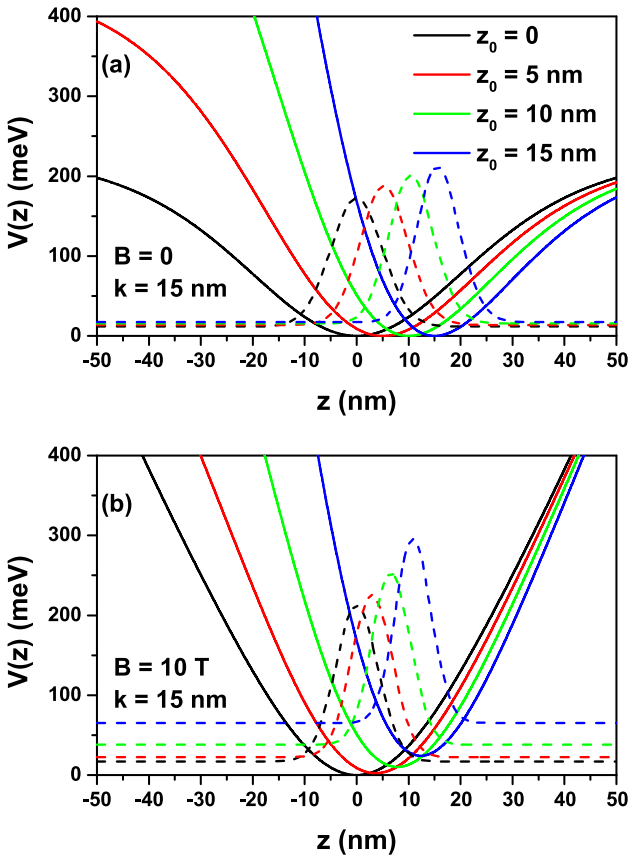


**Fig. 1** For $k = 15\,nm$ and different $z_0$-values, quantum well profiles which have the exponential Rosen–Morse confinement potential, and squared wave functions corresponding to the ground state of the electron localized within the well as a function of the $z$-growth direction coordinate: for $B = 0$ (**a**) and $B = 10$ T (**b**)

### 3.1 The exponential Rosen–Morse potential

In the absence and presence of the magnetic field, the changes in the shape of eRMQW according to the $z_0$ asymmetry parameter as a function of the $z$-coordinate are given in Fig. 1a and b, respectively. When the parameter-$z_0$ is zero, the structure has a symmetrical character, whereas if $z_0$ is nonzero, it becomes an asymmetrical character, and the parameter-$z_0$ also has a dominant effect on geometric confinement. As shown in Fig. 1a, as $z_0$ increases, the minimum point of the potential shifts and barrier height on the right side slowly decreases, while the left side becomes sharper and rises to infinity. So, we defined as an asymmetry parameter the $z_0$ since it causes the eRMQW to turn into an asymmetrical structure. Figure 1b shows the magnetic field effect on the eRMQW structure. The magnetic field creates additional parabolic confinement on QW due to the second term in Eq. (2), so the almost parabolic eRMQW structure, whose minimum slowly shifts toward higher energies, is obtained.

In the absence and presence of the magnetic field, the variations of the energies corresponding to the first three levels of a confined electron within the eRMQW as a function of $z_0$-parameter for $k = 15\,nm$ and $k = 25\,nm$ are given in Fig. 2a and b. Solid (dashed) lines are for $B = 0$ ($B = 10\,T$). For both $B = 0$ and $B = 10\,T$ values of the magnetic field, the energies are an increasing function of $z_0$-parameter since the increase in the $z_0$-parameter causes an increase in the geometric confinement. An increase in the $k$-width parameter weakens the geometric confinement, and therefore, the energies decrease. In the presence of the magnetic field, the energies increase due to magnetic confinement. The energy increase is quite pronounced at large $z_0$-values and in the presence of a magnetic field. As shown from Fig. 1b, the combined effect of the magnetic field and $z_0$-parameter causes a greater increase in geometric confinement rather than individual effects of them. The magnetic field causes a further increase toward the upper energy levels since the right side barrier of the eRMQW also rises sharply to infinity as on the left.

The variations of the energy differences between the energy levels of interest as a function of $z_0$-parameter for both $k = 15\,nm$ and $k = 25$ values are given in Fig. 3a and b. As a natural consequence of the increase in energies as a function of $z_0$, the energy differences between the pointed-out levels in the figures also increase for both $B = 0$ and $B = 10$ T values of the magnetic field.

Figure 4a and b shows the variation of total ACs for a transition that is called the (1–2) between the ground and first excited states of an electron confined within the eRMQW as a function of the incident photon energy for different $z_0$-values for $k = 15\,nm$ and $k = 25\,nm$, respectively. First of all, it should be noted that for $z_0 = 0$, the eRMQW has a symmetrical character, and so the (1–3) transition between the ground state and the second excited state is forbidden, other than that for all $z_0$-values, all transitions are allowed since the structure is asymmetrical. We would also like to point out that since the amplitude of the absorption peak

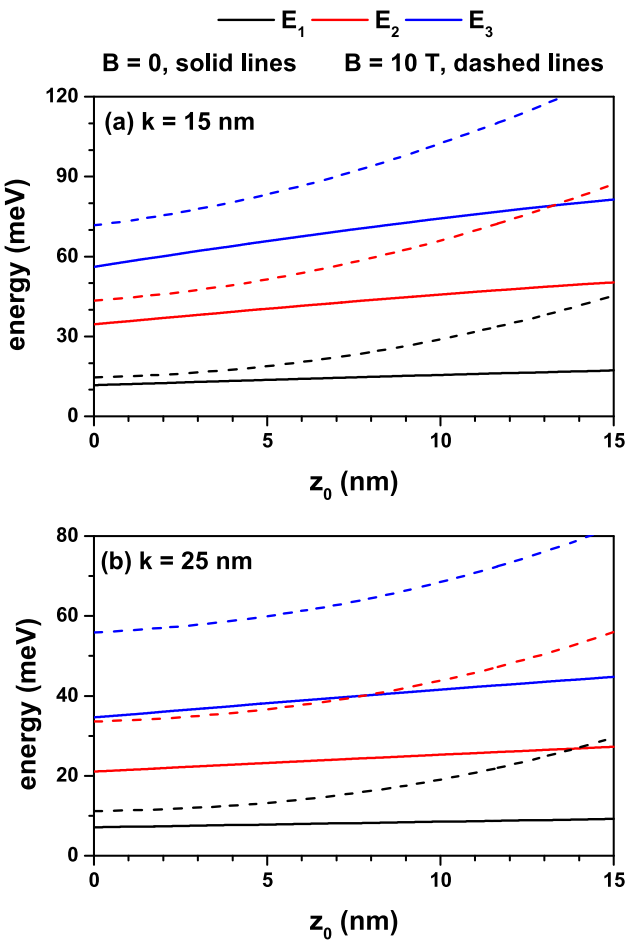


**Fig. 2** The variation of the energies corresponding to the first three energy levels of a confined electron within the exponential Rosen–Morse confinement potential as a function of $z_0$-parameter in the absence and presence of magnetic field: $k = 15\,nm$ (**a**) and $k = 25\,nm$ (**b**). Solid lines (dashed lines) are for $B = 0$ ($B = 10\,T$)

corresponding to this transition is also very small due to the transition matrix element, a figure containing the (1–3) transition is not given.

For $k = 15\,nm$, the total absorption peak positions corresponding to the (1–2) transition shift toward the blue with increasing magnetic field and $z_0$-values. For $k = 25\,nm$, the variation of the absorption peaks for this transition with respect to the magnetic field and $z_0$-parameter is the same, but due to the weakening of the geometric confinement, the absorption peak positions are located at lower photon energies. Furthermore, the bleaching effect that is more pronounced in the weak confinement range is observed in absorption peaks due to the increasing importance of the nonlinear contribution; the contribution of the nonlinear absorption coefficient decreases with increasing the magnetic field and $z_0$-values. This phenomenon occurs when the nonlinear absorption coefficient is much larger than the linear absorption coefficient. It means that the material exhibits a significantly stronger light absorption at high intensities than at low intensities. A significant nonlinear absorption coefficient implies that the material's absorption properties change dramatically with increasing light intensity. The material may exhibit strong absorption or saturation effects at higher light intensities, leading to a higher light attenuation rate. This behavior can be exploited in applications such as optical limiting, optical switching, and nonlinear imaging, where controlling the intensity-dependent absorption is crucial.

As it is known, the energy difference between any two energy levels of interest determines the position of the absorption peaks, and the increase (decrease) in the dipole matrix element determines the increase (decrease) in the absorption peak amplitudes. In this context, to explain the changes in the absorption peak amplitudes in Fig. 5a and b, we present the variation of the reduced dipole matrix element ($\eta_{ij} = M_{ij}/e$) versus the $z_0$-parameter for $k = 15\,nm$ and $k = 25\,nm$, respectively. Solid (dashed) lines are for $B = 0$ ($B = 10\,T$). It should be noted that diagonal (non-diagonal) matrix elements are zero (different zero) $M_{ii} = M_{jj} = 0 (M_{ij} \neq 0)$ in the symmetric case for $z_0 = 0$. As shown in Eqs. (4) and (5), the linear term of AC is proportional to $|M_{ij}|^2$, whereas the third-order nonlinear term of AC is proportional $|M_{ij}|^4$ and also to $|M_{jj} - M_{ii}|^2$. In Fig. 4a and b, a decrease in amplitudes of linear ACs and an increase in amplitudes of nonlinear ACs are observed since $\eta_{12}^2$ decreases slowly with the increasing magnetic field and $z_0$-values, whereas $\eta_{11}^2$ and $\eta_{22}^2$ increase sharply. Therefore, the bleaching effect decreases in the increasing magnetic field and $z_0$-values since the amplitudes of total ACs increase.

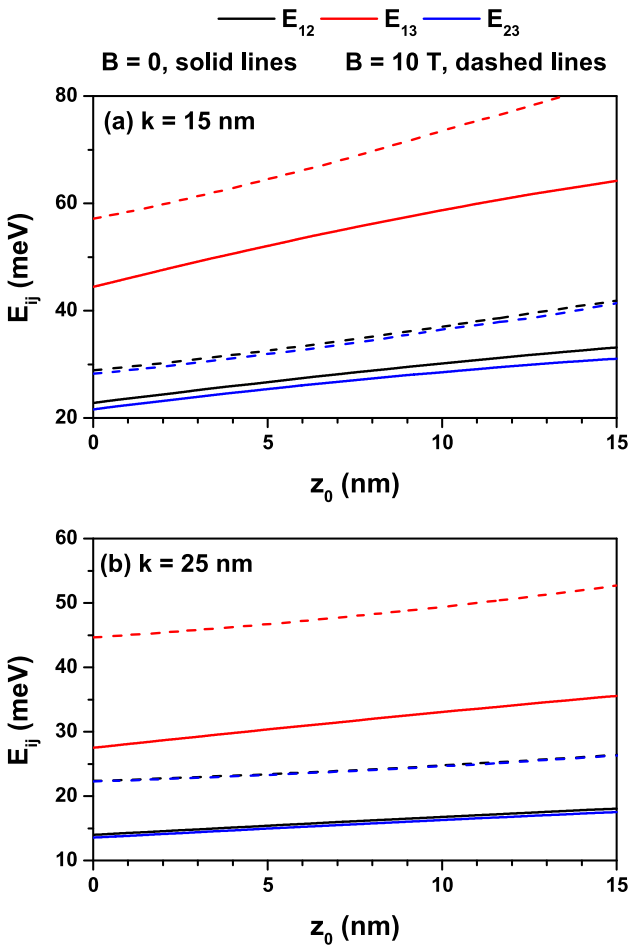


**Fig. 3** The variation of the energy differences between the energy levels of interest as a function of $z_0$-parameter: $k = 15\,nm$ (**a**) and $k = 25\,nm$ (**b**). Solid lines (dashed lines) are for $B = 0$ ($B = 10\,T$)

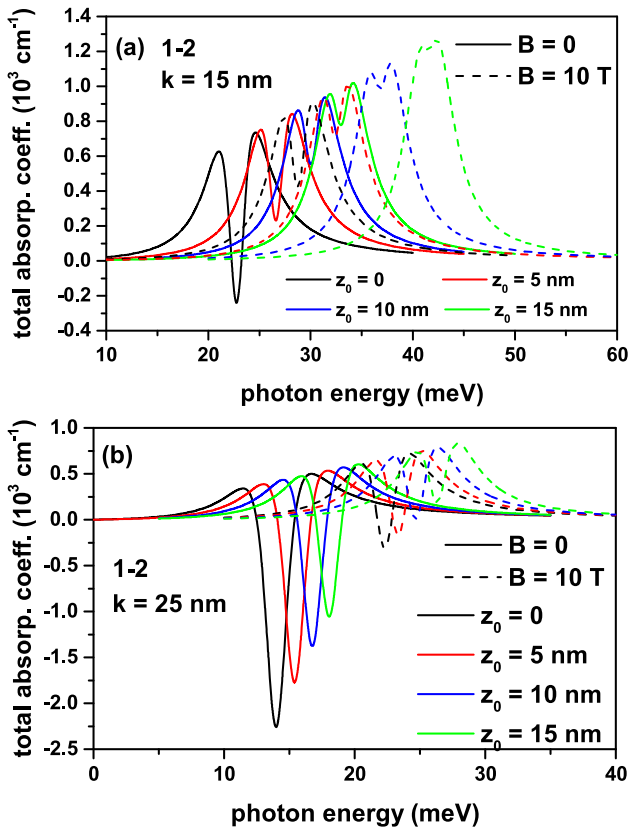


**Fig. 4** The variation of total absorption coefficients for a transition that is called the (1–2) between the ground and first excited states of an electron confined within the quantum well with the exponential Rosen–Morse confinement potential as a function of the incident photon energy for different $z_0$-values: $k = 15\,nm$ (**a**) and $k = 25\,nm$ (Rosen–Morse). Solid lines (dashed lines) are for $B = 0$ ($B = 10\,T$)

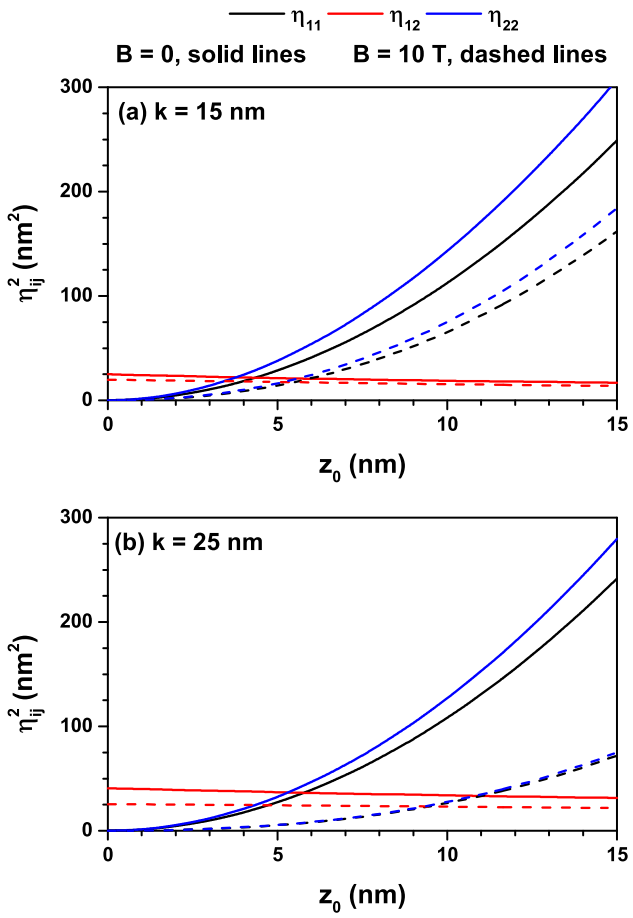


**Fig. 5** In the absence and presence of the magnetic field, the variation of the reduced dipole matrix element ($\eta_{ij} = M_{ij}/e$) versus the $z_0$-parameter: $k = 15\,nm$ (**a**) and $k = 25\,nm$ (**b**). Solid lines (dashed lines) are for $B = 0$ ($B = 10\,T$)

### 3.2 The hyperbolic Rosen–Morse potential

To make comparison both qualitatively and quantitatively the eRMQW and hyperbolic RMQW (hRMQW) potentials, we also took into account the hRMQW confinement potential, which has the following form

$$V^{hRMQW}(z) = \frac{V_0}{2}\left[1 - \mathrm{sech}^2(z/k) + \tanh^2(z/k)\right], \tag{7}$$

where $V_0$, $z$, and $k$-parameters are as defined in the eRMQW potential. In order to make a detailed comparison of exponential and hRMQW results, we should also point out that the potential function given in Eq. (6) was developed by us, unlike the one given in the literature [21–23].

As shown in Figs. 1 and 6 and (for $z_0 = 0$), both the QWs have the same shape, for hRMQW, only the $k$-width parameter can be changed, and its symmetry can be broken by applying an external electric field. However, as shown from Eq. (2), eRMQW has more tuning parameters than that of hRMQW, and it has an asymmetric character by changing the $z_0$-parameter. As mentioned before, thanks to this degree of freedom, eRMQW is a more reliable and advantageous model, since it provides a more flexible framework for validating experimental data.

The variation of the energies corresponding to the first three levels of confined electron within the eRMQW for $z_0 = 0$ and hRMQW as a function of the applied magnetic field is given in Fig. 7, for $k = 15$ nm. The energies are an increasing function of the magnetic field. Due to having a stronger confinement, energies and also energy intervals corresponding to the hRMQW are larger than those of eRMQW.

Figure 8 shows the variation of the energy differences among the first three energy levels versus the magnetic field. For both models, the energy differences between the levels we are interested in are increasing functions of the magnetic field. Energy differences for hRMQW are also larger than those for eRMQW. These results mean that the absorption peaks of hRMQW will be located at higher photon energies than those of eRMQW.

For both eRMQW and hRMQW, the linear, nonlinear, and total ACs corresponding to the (1–2) transition as a function of the incident photon energy for different magnetic field values are given in Fig. 9. Dashed, dotes, and solid lines are for the linear, nonlinear, and total ACs. The black, red, blue, and green lines are for $B = 0$, 10 T, 15 T, and 20 T, respectively. As shown in Fig. 9, in both models, the AC peaks blue shift with increasing magnetic field; note that the absorption peaks corresponding to the hRMQW

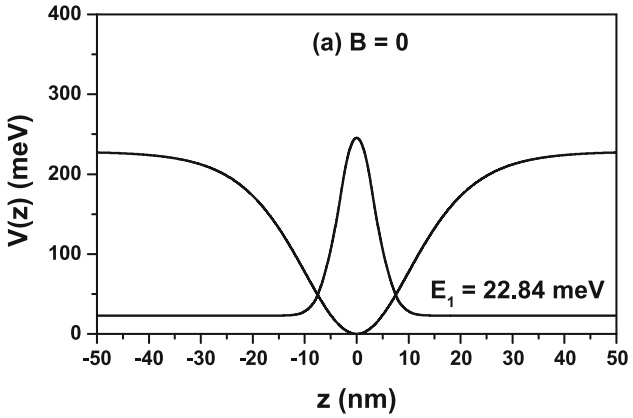


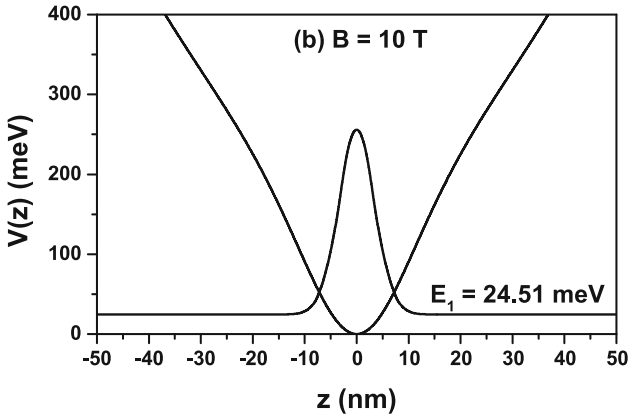


**Fig. 6** For $k = 15\,nm$, the quantum well profiles, which have the hyperbolic Rosen–Morse confinement potential, and the squared wave functions corresponding to the ground state of the electron localized within the well as a function of the $z$-growth direction coordinate. Results are for $B = 0$ (**a**) and $B = 10$ T (Rosen–Morse). The corresponding ground state eigenvalues are indicated

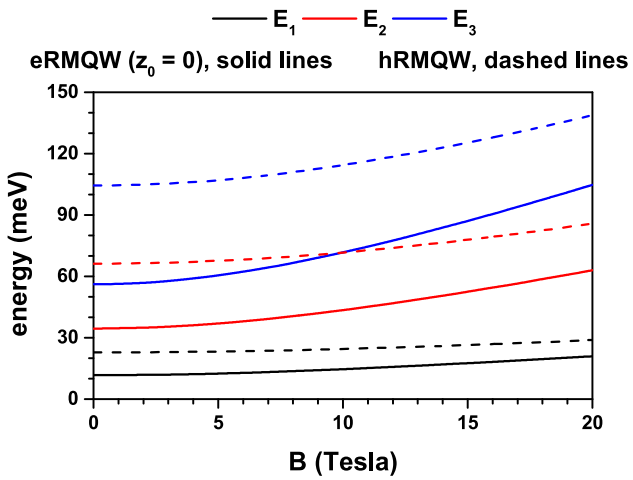


**Fig. 7** The variation of the energies corresponding to the first three energy levels of a confined electron within the exponential (solid lines) and hyperbolic (dashed lines) Rosen–Morse confinement potential as a function of the applied magnetic field. In the case of the exponential Rosen–Morse, calculations are for $z_0 = 0$

are localized at higher photon energies than those for eRMQW. While the amplitude of the linear AC almost does not change with the effect of the magnetic field, the amplitude of the nonlinear AC decreases, and thus, the bleaching effect decreases, and gradually, the bleaching effect begins to disappear. In the hRMQW model, as the energy intervals and also $E_{12}$ are larger than that of eRMQW, the bleaching effect is very weak, and at $B = 15$ T, the bleaching effect is no longer observed.

## 4 Conclusions

In this study, we investigated the electronic and optical properties of the exponential Rosen–Morse quantum well under the effects of an applied magnetic field, which is applied parallel to the growth direction of the structure considered. To the best of our knowledge, this potential has not yet been used to investigate low-dimensional systems' electronic and optical properties, except for calculating the rotational vibration energies of some diatomic molecules. Furthermore, in order to make a detailed comparison with

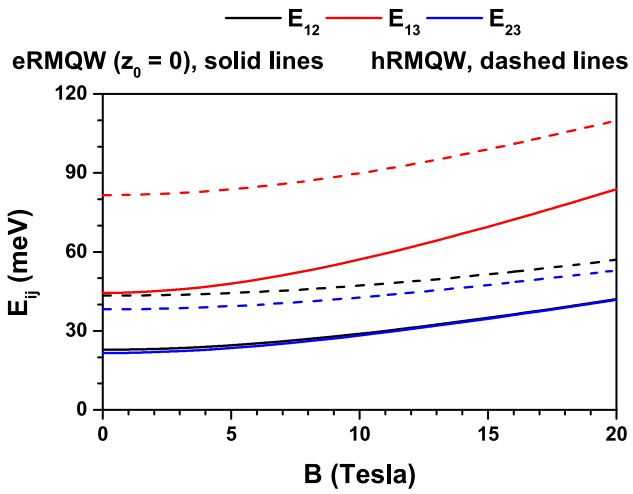


**Fig. 8** The variation of the energy differences between the energy levels of interest of a confined electron within the exponential (solid lines) and hyperbolic (dashed lines) Rosen–Morse confinement potential as a function of the applied magnetic field. In the case of the exponential Rosen–Morse, calculations are for $z_0 = 0$

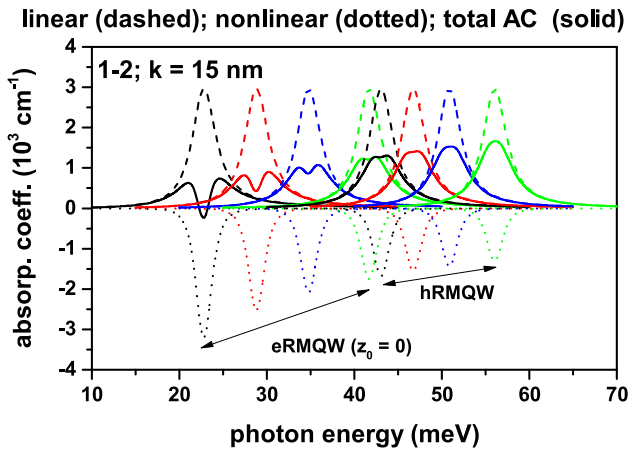


**Fig. 9** The variation of lineal, nonlinear, and total absorption coefficients for a transition that is called the (1–2) between the ground and first excited states of an electron confined within the quantum well with the exponential and hyperbolic Rosen–Morse confinement potential as a function of the incident photon energy for different magnetic field values (for each potential, from left to right, the magnetic field values are $B = 0$, 10 T, 15 T, and 20 T). For the exponential Rosen–Morse potential, the calculations are with $z_0 = 0$

the hyperbolic RMQW potential, we compared the results we obtained using the same parameter values for the hRMQW potential modified by us. The magnetic field, asymmetry, and confinement parameters lead to a significant increase electron energies, energy differences between the confined electron states, and a blue shift in the absorption spectrum. Energies and energy differences between the energy levels which are considered for hRMQW are also larger than those for eRMQW. Thus, the absorption peaks of hRMQW shift to higher photon energies than those of eRMQW. It should be noted that a blue shift is also observed in the absorption peaks corresponding to the eRMQW with the zo parameter.

The blue shift of the absorption peaks can be advantageous for applications such as optoelectronics and photonics. By controlling the blue shift, researchers can engineer the bandgap of low-dimensional materials to tailor their optical and electronic properties for specific device applications. The blue shift of an absorption peak is an important phenomenon in many areas of science and technology, including materials science, chemistry, and optics. It can probe the electronic and structural properties of materials and develop new materials with tailored optical properties.

**Acknowledgements** CAD is grateful to Colombian agencies CODI-Universidad de Antioquia (Estrategia de Sostenibilidad de la Universidad de Antioquia and projects "Propiedades magneto-ópticas y óptica no lineal en superredes de Grafeno," "Estudio de propiedades ópticas en sistemas semiconductores de dimensiones nanoscópicas," "Propiedades de transporte, espintrónicas y térmicas en el sistema molecular ZincPorfirina," and "Complejos excitónicos y propiedades de transporte en sistemas nanométricos de semiconductores con simetría axial") and Facultad de Ciencias Exactas y Naturales-Universidad de Antioquia (CAD exclusive dedication project 2022-2023).

**Author contributions** The contributions of the authors are as follows: EK worked on the numerical calculations, in formal analysis, and writing of the manuscript. MBY worked on the formal analysis and writing of the manuscript. CAD worked on the numerical calculations and writing of the manuscript.

**Funding** Open Access funding provided by Colombia Consortium.

**Data Availability Statement** This manuscript has associated data in a data repository. [Authors' comment: All the files with tables, figures, and codes are available. The corresponding author will provide all the files in case they are requested.]

**Declarations**

**Conflict of interest** The authors do not have any financial and non-financial competing interests statement.



## References

1. G. Vignesh, P. Nithiananthi, Effect of confinement potential on exciton diamagnetism in the perspective of constituent carriers in a quantum well. J. Phys. Chem. Sol. **114**, 187–194 (2018). https://doi.org/10.1016/j.jpcs.2017.11.003
2. W. Xie, Two interacting electrons in a spherical Gaussian confining potential quantum well. Commun. Theor. Phys. **42**, 151–154 (2004). https://doi.org/10.1088/0253-6102/42/1/151
3. M.G. Barseghyan, A.A. Kirakosyan, Electronic states in a step quantum well in a magnetic field. Physica E **28**, 471–481 (2005). https://doi.org/10.1016/j.physe.2005.05.058
4. J.A. Gil-Corrales, A.L. Morales, C.A. Duque, Self-consistent study of GaAs/AlGaAs quantum wells with modulated doping. Nanomaterials **13**, 913 (2023). https://doi.org/10.3390/nano13050913
5. F. Barreto-Basave, M.E. Mora-Ramos, F. Ungan, I. Pérez-Quintana, C.A. Duque, Fibonacci hyperbolic quantum wells: a model for two-level non-linear optical response. Opt. Quant. Electron. **55**, 87 (2023). https://doi.org/10.1007/s11082-022-04370-8
6. İ Karabulut, Ü. Atav, H. Şafak, M. Tomak, Linear and nonlinear intersubband optical absorptions in an asymmetric rectangular quantum well. Eur. Phys. J. B **55**, 283–288 (2007). https://doi.org/10.1140/epjb/e2007-00055-1
7. E. Kasapoglu, C.A. Duque, Position dependent effective mass effect on the quantum wells with three-parameter modified Manning potential. Optik **243**, 166840 (2021). https://doi.org/10.1016/j.ijleo.2021.166840
8. H. Sari, F. Ungan, E. Kasapoglu, S. Sakiroglu, I. Sökmen, Intense laser-induced electronic and optical properties in double finite oscillator potential. Phil. Mag. **99**, 2444–2456 (2019). https://doi.org/10.1080/14786435.2019.1617907
9. S. Baskoutas, C. Garoufalis, A.F. Terzis, Linear and nonlinear optical absorption coefficients in inverse parabolic quantum wells under static external electric field. Eur. Phys. J. B **84**, 241–247 (2011). https://doi.org/10.1140/epjb/e2011-20470-9
10. E. Kasapoglu, Binding energy of donor impurities in double inverse parabolic quantum well under electric field. Physica E **41**, 1222–1225 (2009). https://doi.org/10.1016/j.physe.2009.02.003
11. C.A. Duque, M.E. Mora-Ramos, E. Kasapoglu, H. Sari, I. Sökmen, Combined effects of intense laser field and applied electric field on exciton states in GaAs quantum wells: transition from the single to double quantum well. Phys. Status Solidi (B) **249**, 118–127 (2012). https://doi.org/10.1002/pssb.201147250
12. E. Kasapoglu, I. Sökmen, Interband absorption and exciton binding energy in an inverse parabolic quantum well under the magnetic field. Phys. Lett. A **372**, 56–59 (2007). https://doi.org/10.1016/j.physleta.2007.06.072
13. E. Kasapoglu, F. Ungan, C.A. Duque, U. Yesilgul, M.E. Mora-Ramos, H. Sari, I. Sokmen, The effects of the electric and magnetic fields on the nonlinear optical properties in the step-like asymmetric quantum well. Physica E **61**, 107–110 (2014). https://doi.org/10.1016/j.physe.2014.03.024
14. Z.-H. Zhang, L. Zou, K.-X. Guo, J.-H. Yuan, The nonlinear optical rectification in asymmetrical and symmetrical Gaussian potential quantum wells with applied electric field. Opt. Commun. **359**, 316–321 (2016). https://doi.org/10.1016/j.optmat.2016.01.043
15. A. Keshavarz, M.J. Karimi, Linear and nonlinear intersubband optical absorption in symmetric double semi-parabolic quantum wells. Phys. Lett. A **374**, 2675–2680 (2010). https://doi.org/10.1016/j.physleta.2010.04.049
16. S. Baskoutas, C. Garoufalis, A.F. Terzis, Linear and nonlinear optical absorption coefficients in inverse parabolic quantum wells under static external electric field. Eur. Phys. J. B **84**, 241–247 (2011). https://doi.org/10.1140/epjb/e2011-20470-9
17. A. AL-Naghmaish, H. Dakhlaoui, T. Ghrib, B. M. Wong, Effects of magnetic, electric, and intense laser fields on the optical properties of AlGaAs/GaAs quantum wells for terahertz photodetectors. Physica B **635**, 413838 (2022). https://doi.org/10.1016/j.physb.2022.413838
18. H. Dakhlaoui, M. Nefzi, Tuning the linear and nonlinear optical properties in double and triple $\delta$ doped GaAs semiconductor: impact of electric and magnetic field. Superlattice. Microst. **136**, 106292 (2019). https://doi.org/10.1016/j.spmi.2019.106292
19. H. Dakhlaoui, W. Belhadj, F. Ungan, N.S. Al-Shameri, Linear and nonlinear optical properties in GaAs quantum well based on konwent-like potential: effects of impurities and structural parameters. Physica E **152**, 115760 (2023). https://doi.org/10.1016/j.physe.2023.115760
20. E. Kasapoglu, C.A. Duque, Position dependent effective mass effect on the quantum wells with three-parameter modified Manning potential. Optik **243**, 166840 (2021). https://doi.org/10.1016/j.ijleo.2021.166840
21. A. Salman Durmuslar, A. Turkoglu, M.E. Mora-Ramos, F. Ungan, The non-resonant intense laser field effects on the binding energies and the nonlinear optical properties of a donor impurity in Rosen-Morse quantum well. Indian J. Phys. **96**, 3485–3492 (2022). https://doi.org/10.1007/s12648-021-02251-6
22. F. Ungan, M.K. Bahar, The laser field controlling on the nonlinear optical specifications of the electric field-triggered Rosen-Morse quantum well. Phys. Lett. A **384**, 126400 (2020). https://doi.org/10.1016/j.physleta.2020.126400
23. R. Khordad, B. Mirhosseini, Linear and nonlinear optical properties in spherical quantum dots: Rosen-Morse potential. Opt. Spectrosc. **117**, 434 (2014). https://doi.org/10.1016/j.physleta.2021.127262
24. E. Kasapoglu, H. Sari, I. Sökmen, J.A. Vinasco, D. Laroze, C.A. Duque, Effects of intense laser field and position dependent effective mass in Razavy quantum wells and quantum dots. Physica E **126**, 114461 (2021). https://doi.org/10.1016/j.physe.2020.114461
25. C.S. Jia, Y.F. Diao, X.J. Liu, P.Q. Wang, J.Y. Liu, G.D. Zhang, Equivalence of the Wei potential model and Tietz potential model for diatomic molecules. J Chem Phys **137**, 014101 (2012). https://doi.org/10.1063/1.4731340
26. N. Zeiri, N. Sfina, S. Abdi-BenNasrallah, M. Said, Linear and non-linear optical properties in symmetric and asymmetric double quantum wells. Optik **124**, 7044–7048 (2013). https://doi.org/10.1016/j.ijleo.2013.05.169
27. N. Dinh Hien, Comparison of the nonlinear optical properties of asymmetrical and symmetrical quantum wells. The Eur. Phys. J. B **95**, 192 (2022). https://doi.org/10.1140/epjb/s10051-022-00455-1